JPhys Photonics

Flexible photonic devices based on dielectric antennas

View the article online for updates and enhancements.

JPhys Photonics

PAPER

Flexible photonic devices based on dielectric antennas

Abdennacer Benali[1] , Jean-Benoît Claude[2], Nicoletta Granchi[1,3,4], Simona Checcucci[1,3,4], Mohammed Bouabdellaoui[1,5] , Mimoun Zazoui[5] , Monica Bollani[6] , Marco Salvalaglio[7] , Jérôme Wenger[2], Luc Favre[1] , David Grosso[1], Antoine Ronda[1], Isabelle Berbezier[1], Massimo Gurioli[1,3] and Marco Abbarchi[1]

1   Aix Marseille Univ, Université de Toulon, CNRS, IM2NP, Marseille, France
2   Aix Marseille Univ, CNRS, Centrale Marseille, Institut Fresnel, Marseille, France
3   Dipartimento di Fisica ed Astronomia Universitá degli Studi di Firenze, I-50019 Sesto Fiorentino, Italy
4   European Laboratory for Nonlinear Spectroscopy (LENS), I-50019 Sesto Fiorentino, Italy
5   Laboratory of Physics of Condensed Matter and Renewable Energy, Faculty of Sciences and Technology, Hassan II University of Casablanca, 146 Mohammedia, Morocco
6   Istituto di Fotonica e Nanotecnologie-Consiglio Nazionale delle Ricerche, Laboratory for Nanostructure Epitaxy and Spintronics on Silicon, LNESS, Via Anzani 42, I-22100 Como, Italy
7   Institute of Scientific Computing, Technische Universität Dresden, D-01062 Dresden, Germany

E-mail: marco.abbarchi@im2np.fr

Abstract

Flexible and stretchable photonics are emerging fields aiming to develop novel applications where the devices need to conform to uneven surfaces or whenever lightness and reduced thickness are major requirements. However, owing to the relatively small refractive index of transparent soft matter including most polymers, these materials are not well adapted for light management at visible and near-infrared frequencies. Here we demonstrate simple, low cost and efficient protocols for fabricating $Si_{1-x}Ge_x$-based, sub-micrometric dielectric antennas over record scales (50 mm wafers) with ensuing hybrid integration into different plastic supports. The transfer process has a near-unity yield: up to 99.94% for disordered structures and 99.5% for the ordered counterpart. Finally, we benchmark the optical quality of the dielectric antennas with light scattering measurements, demonstrating the control of the islands structural color and the onset of sharp Mie modes after encapsulation in plastic. Thanks to the ease of implementation of our fabrication methods, these results are relevant for the integration of SiGe-based dielectric Mie resonators in flexible substrates over large surfaces.

1. Introduction

Flexible devices on plastic bring transformational advantages including shapeability, stretchability, lightness and limited thickness, providing unique solutions to novel and old problems [1–8]. The simplest exploitation concerns applications where the device should conform to complex surfaces or needs to bend, such as folding mobile-phones. More complex architectures [9, 10], such as in case of tightly assembled packages, would also benefit from multiple stacks of flexible, light and foldable chips. Stretchable photonic circuits [11, 12] are ideal for strain sensors and gauges, where they join the need to adapt the device to the uneven and warping surfaces and the well-known sensitivity of photonic resonances to small deformations [13–16]. Photodetectors [17], structural color change [5], endoscopic lenses [18] are further examples of relevant applications of bendable and stretchable devices.

Polymers and other soft materials have been extensively studied for flexible photonics via nanoimprinting, direct laser writing, and 3D printing [19, 20]. Still, all these results are inherently limited by the low index of refraction of any soft material, reducing the light confinement and the strength of the photonic resonances with respect to inorganic semiconductor-based platforms (e.g. Si [21] or InP [22] photonics). At the same time, these

latter materials pay their superior photonic response with bulky and rigid devices not adapted to flexible photonic applications.

In order to bridge plastic supports with inorganic semiconductor photonic systems, several hybrid approaches have been proposed, in the last decade [1, 2]. These processes have been exploited for several applications (e.g. transparent electronics [1–3], bio-integrated devices [4], sensing [8] and photonics [23–25]) enjoying several advantages offered by organic supports, including their low per-area weight, low cost, flexibility, elasticity, bio-compatibility, and optical transparency.

Here we join the simplicity and low cost of solid state dewetting [26] of ultra-thin Si, SiGe and Ge films on SiO$_2$ for the fabrication of sub-micrometric dielectric Mie resonators [27] over record-scales (50 mm diameter wafers) with two distinct and efficient protocols for encapsulating them into flexible and transparent, organic supports. The first method is based on bendable perfluoropolyether-urethane dimethacrylate (PFPE, MD-700), which is reticulated under UV illumination at room temperature and is better suited for applications where no annealing is possible and for further transfer of the structures (e.g. on a glass window). The second method employs polydimethylsiloxane (PDMS) which, in addition to bending to extreme angles, is stretchable. In both cases, the Si$_{1-x}$Ge$_x$ particles remain embedded in the cross-linked polymer and can be easily peeled from the original substrate with an extremely high yield (larger than 99%). We assess the performances of the protocols for self assembled sub-micrometric antennas from spontaneously dewetted Si$_{1-x}$Ge$_x$ films and for pre-patterned samples leading to ordered and custom-designed metasurfaces. Optical experiments are used to asses the optical quality of our flexible photonic devices.

2. Experimental methods

2.1. Panorama of different dewetting scenarios

The ultra-thin silicon films on insulator (UT-SOI, from Soitec), are single-crystal (001) oriented films, 12 nm thick, bonded to a 25 nm thick SiO$_2$ layer (buried oxide, BOX) on a Si (001) wafer. Custom-made, ultra-thin silicon (-germanium) films on insulator (S(G)OI) are obtained by rapid thermal oxidation (RTO) at 950 °C in O$_2$ atmosphere for 2 h (in a furnace from Jipelec) followed by Si$_{1-x}$Ge$_x$ deposition in a molecular beam epitaxy reactor (MBE from Riber, static ultra-high vacuum $\sim 10^{-10}$ Torr). The thin Si$_{1-x}$Ge$_x$ layers are first cleaned with an annealing flash at 600 °C for 30′ and then annealed between 620 °C and 800 °C for 1–4 h in order to induce the dewetting [27–30]. Templated dewetting is obtained by etching the UT-SOI via e-beam lithography and reactive ion etching (EBL and RIE) prior to annealing [31].

We first describe several solid-state dewetting processes illustrating the versatility of this approach in producing a plethora of different scenarios of islands size, density, shape and composition (figure 1). Generally speaking, the common steps to all the samples are a first chemical cleaning in a HF solution (5% HF in deionized water) in a glow box under N$_2$ atmosphere. This step is necessary to remove any residual native oxide from the sample surface which perturbs the surface atoms mobility and has a detrimental effect on the dewetting process (figure 1(a)). The samples are then transferred in a molecular beam reactor (MBE) under ultra-high vacuum ($\sim 10^{-10}$ Torr) where they undergo a temperature flash (typically at 600 °C) in order to further remove any trace of native oxide. This step is thus followed by dewetting at high temperature (700 °C–800 °C) and eventually SiGe deposition (figure 1(b)).

As a first example of island formation, a commercial, monocrystalline UT-SOI can be dewetted to form monocrystalline Si-based islands, which, for this initial Si thickness (12 nm), have a lateral size ranging from 150 to 400 nm and a height from 60 to 120 nm (figure 1(c), second panel) [27, 28]. Starting from the same initial wafer, size, shape and composition of the islands can be engineered by adding before annealing, several nm of Si$_{1-x}$Ge$_x$ atop the pristine UT-SOI via MBE (figure 1(c), third panel). For 20 nm of SiGe deposition (30% Ge) the islands have a base ranging from 0.5 up to 1 μm.

A control over the spatial distribution and density of the islands is obtained in two fabrication steps: first by partially dewetting a commercial UT-SOI and, after turning off the heating, by adding a few monolayers of Ge (figure 1(c), fourth panel) [28, 32]. This process results in a bi-modal size distribution of large, Si-rich islands (base size from 250 up to 500 nm) and small, Ge-rich islands (base size from 200 up to 300 nm). In contrast with the previous case, large and small islands can be perfectly mixed together by adding Ge during the annealing step (figure 1(c), fifth panel) [33].

A convenient alternative way for the fabrication of Si$_{1-x}$Ge$_x$ islands exploits custom-made S(G)OI (figure 1(d)) [34]. In this case, a Si wafer is first processed by RTO forming an arbitrarily thick thermal oxide (e.g. 130 nm in this work), SiGe deposition by MBE and finally, annealing.

A last example is templated dewetting of UT-SOI (figure 1(e)): [27, 29, 31, 34, 35] by etching a commercial UT-SOI (figure 1(e), first panel) with patches of well defined size and spacing and eventually adding other features (e.g. pits and holes) the annealing provides ordered arrays of individual islands (figure 1(e), second to
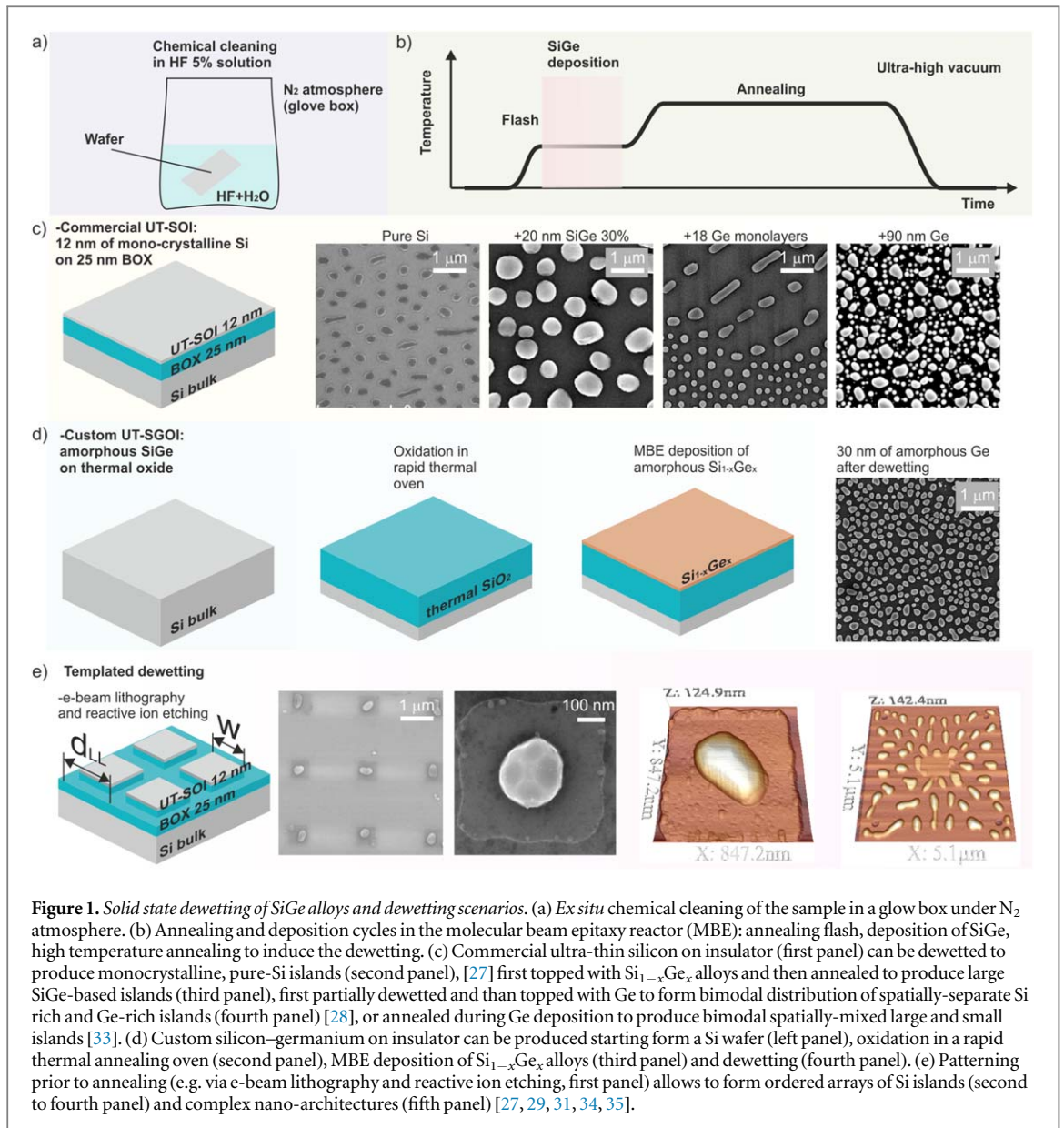
Figure 1. *Solid state dewetting of SiGe alloys and dewetting scenarios.* (a) *Ex situ* chemical cleaning of the sample in a glow box under N_2 atmosphere. (b) Annealing and deposition cycles in the molecular beam epitaxy reactor (MBE): annealing flash, deposition of SiGe, high temperature annealing to induce the dewetting. (c) Commercial ultra-thin silicon on insulator (first panel) can be dewetted to produce monocrystalline, pure-Si islands (second panel), [27] first topped with $Si_{1-x}Ge_x$ alloys and then annealed to produce large SiGe-based islands (third panel), first partially dewetted and than topped with Ge to form bimodal distribution of spatially-separate Si rich and Ge-rich islands (fourth panel) [28], or annealed during Ge deposition to produce bimodal spatially-mixed large and small islands [33]. (d) Custom silicon–germanium on insulator can be produced starting form a Si wafer (left panel), oxidation in a rapid thermal annealing oven (second panel), MBE deposition of $Si_{1-x}Ge_x$ alloys (third panel) and dewetting (fourth panel). (e) Patterning prior to annealing (e.g. via e-beam lithography and reactive ion etching, first panel) allows to form ordered arrays of Si islands (second to fourth panel) and complex nano-architectures (fifth panel) [27, 29, 31, 34, 35].

fourth panel), complex assemblies of islands [29, 34] (figure 1(e), fifth panel) and complex nano-architectures [31, 35].
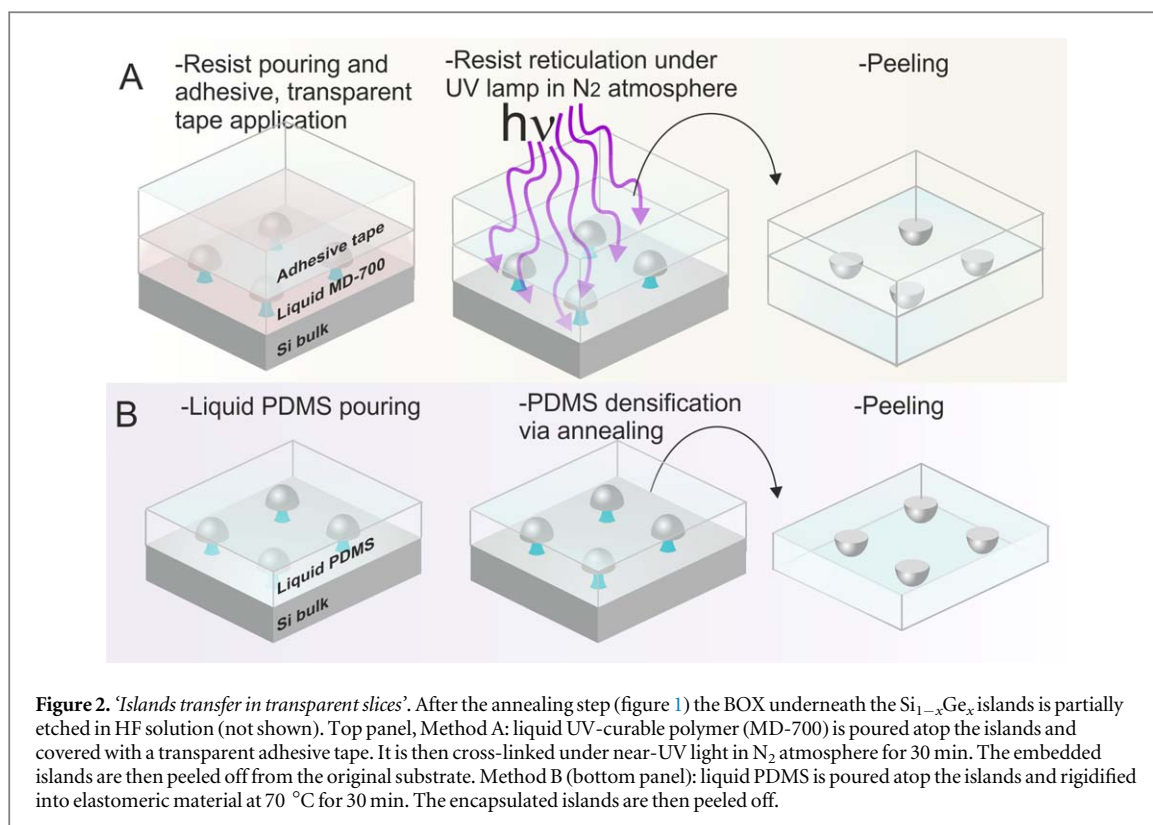
It emerges that via solid state dewetting, we can create many different kind of dielectric islands tuning their size, shape, composition, density, and spatial organization, eventually obtaining highly homogeneous and ordered arrays. On the other side, the possible uses of dewetting are limited by the presence of a rigid, bulky and non-transparent substrate. Thus, a full exploitation of this method for nano-photonics requires further processing in order to release the islands from their original support allowing for instance, their use for light transmission.

2.2. Nano-transfer on transparent substrates

Two alternative procedures (method A and B) are exploited in order to transfer the dewetted islands in transparent supports (figure 2) [11, 12]. They both involve a common etching step (not shown) for partially removing the BOX by dipping the samples in a solution of HF for 10–30 min (as discussed hereafter) and then rinsing the sample by de-ionized water.

Method A is based on MD-700 (from Solway) UV-curable polymer (figure 2 top panels). By pouring it on the dewetted islands after HF attack and covering with a transparent and adhesive plastic foil (Adwill D series UV-curable dicing tape from Lintec), the polymer is rigidified placing the ensemble for 30 min in N_2 atmosphere and exposing it to a LED emitting at ~365 nm (from Spectroline). Finally the encapsulated islands are peeled-off.

Method B is based on PDMS (figure 2, bottom panels): it is implemented by directly pouring the mixed PDMS reactants (90% RTV141A and 10% RTV141B from BLUESIL) onto the samples (after HF attack),

Figure 2. '*Islands transfer in transparent slices*'. After the annealing step (figure 1) the BOX underneath the $Si_{1-x}Ge_x$ islands is partially etched in HF solution (not shown). Top panel, Method A: liquid UV-curable polymer (MD-700) is poured atop the islands and covered with a transparent adhesive tape. It is then cross-linked under near-UV light in N_2 atmosphere for 30 min. The embedded islands are then peeled off from the original substrate. Method B (bottom panel): liquid PDMS is poured atop the islands and rigidified into elastomeric material at 70 °C for 30 min. The encapsulated islands are then peeled off.

pumping under primary vacuum and finally cross-linking at 70 °C in an oven (from Binder) for 30 min under room atmosphere. Thus, after the solidification of the PDMS, the embedded islands can be peeled off.
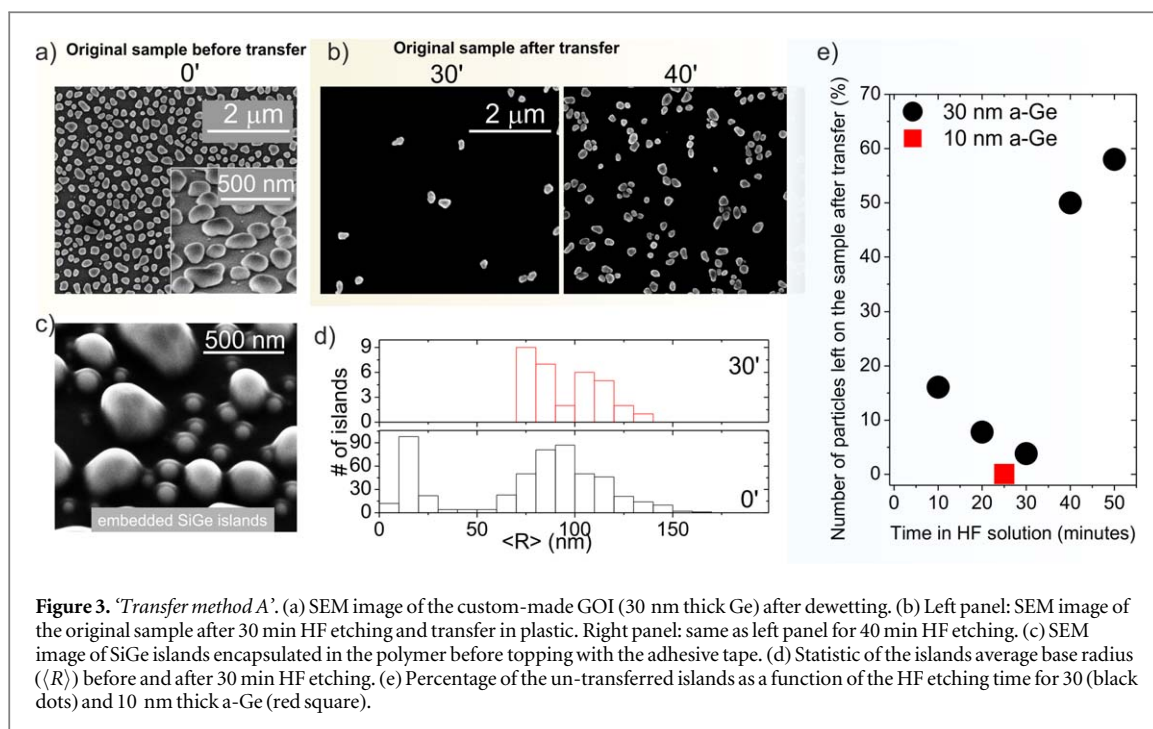
2.3. Samples characterization

The samples are characterized by atomic force microscopy in non-contact mode (AFM, PSIA XE-100 AFM) and scanning electron microscopy (SEM, Dual-beam FIB HELIOS nanolab). Dark-field (DF) spectra are obtained via confocal spectroscopic microscopy coupling a commercial Zeiss microscope with a spectrometer and Si-based CCD linear array (Flame-T-VIS–NIR by Ocean Optics) through an optical fiber (Ocean Optics multimode fiber, vis–NIR, core diameter 200 μm). DF microscope images and spectra are obtained by shining white LED light with a ~70° angle with respect to the sample surface. Resonant light scattering [27] is collected by a high numerical aperture (NA = 0.75) 50× magnification objective lens (lateral resolution ~400 nm in imaging and of ~2 μm in spectroscopy). Images are registered with a color CCD camera. Reflectance spectra at quasi-normal incidence are obtained with a spectrophotometer (from Perkin Elmer) mounting an integrating sphere.

3. Method A: transfer of spontaneously dewetted islands from 50 mm wafers

In order to illustrate the transfer process based on method A, we take into account a custom UT-GOI. This is obtained by processing a 50 mm Si wafer by (1) RTO, forming a 130 nm thick thermal oxide, (2) Ge deposition (10 and 30 nm) by MBE and finally, annealing at high temperature (as in figure 1(d)). Owing to the amorphous nature of the initial UT-GOI, after dewetting the islands are poly-crystalline and their shape rather irregular (as in figure 3(a)).

This sample is diced in 6 parts in order to study the effect of etching on the efficiency of the transfer process. We perform a systematic investigation of the efficiency of the transfer process for 10–50 min HF etching assessing the yield of the transfer process monitoring the number of un-transferred particles left on the original substrate (figure 3(b)). We observe a decreasing trend of the number of un-transferred islands up to a minimum of ~4% for 30′ etching (figure 3(e)) whereas longer etching time provides a much less performing transfer. For a 10 nm thick a-Ge layer and 25′ HF etching, we were able to obtain even better results with a transfer yield as large as 99.94%.

We also monitor the size of the particles before and after HF etching. for an initial UT-GOI of 30 nm a-Ge before HF etching, the average radius of the particles $\langle R \rangle$ has a bimodal statistical distribution with a peak at about 17 nm and a second one at 95 nm (figure 3(d), bottom panel). After 30 min etching and transfer, the smaller particles are missing from the original wafer and the larger ones are, to a first approximation, distributed

Figure 3. '*Transfer method A*'. (a) SEM image of the custom-made GOI (30 nm thick Ge) after dewetting. (b) Left panel: SEM image of the original sample after 30 min HF etching and transfer in plastic. Right panel: same as left panel for 40 min HF etching. (c) SEM image of SiGe islands encapsulated in the polymer before topping with the adhesive tape. (d) Statistic of the islands average base radius ($\langle R \rangle$) before and after 30 min HF etching. (e) Percentage of the un-transferred islands as a function of the HF etching time for 30 (black dots) and 10 nm thick a-Ge (red square).

as those found on the original sample (figure 3(d), top panel). We conclude that the smaller particles are either removed by the chemical attack or are all encapsulated in the polymer and that the etching process does not modify the size of the Ge particles. This is not obvious owing to the relatively fast oxidation of Ge and the solubility of GeO_x in deionized water.

Aside we note that with this process, the polymer completely embeds the islands with a very thin layer, as accounted for by imaging of densified MD-700 not yet peeled from the original substrate bearing the islands: high-resolution SEM images from a sample bearing large and small SiGe-based islands (not yet transferred) show that the polymer has a thickness of about 35 nm (figure 3(c), bottom panel).

By following the same procedure optimized for small ($\sim cm^2$), custom UT-GOI we extend the process to 50 mm wafers bearing Ge islands formed from 30 to 10 nm a-Ge dewetting (figure 4). Although after transfer we observe some influence of edge effects, the transfer is almost complete for both cases. For the smaller particles we observe a marked structural color in the visible range (figure 4(a), bottom panel) and in all cases, the plastic embedding the islands can be bent to a large curvature.

By monitoring the light diffusion we observe the presence of size-dependent resonances with a peak at about 900 nm for the larger particles obtained from 30 nm a-Ge dewetting, and at 700 nm for the smaller ones from 10 nm a-Ge (figure 4(b), top and bottom panels respectively). These bands are interpreted as multi-polar Mie modes sustained by the particles, as expected for this kind of devices [27, 30, 33, 34, 36–38].
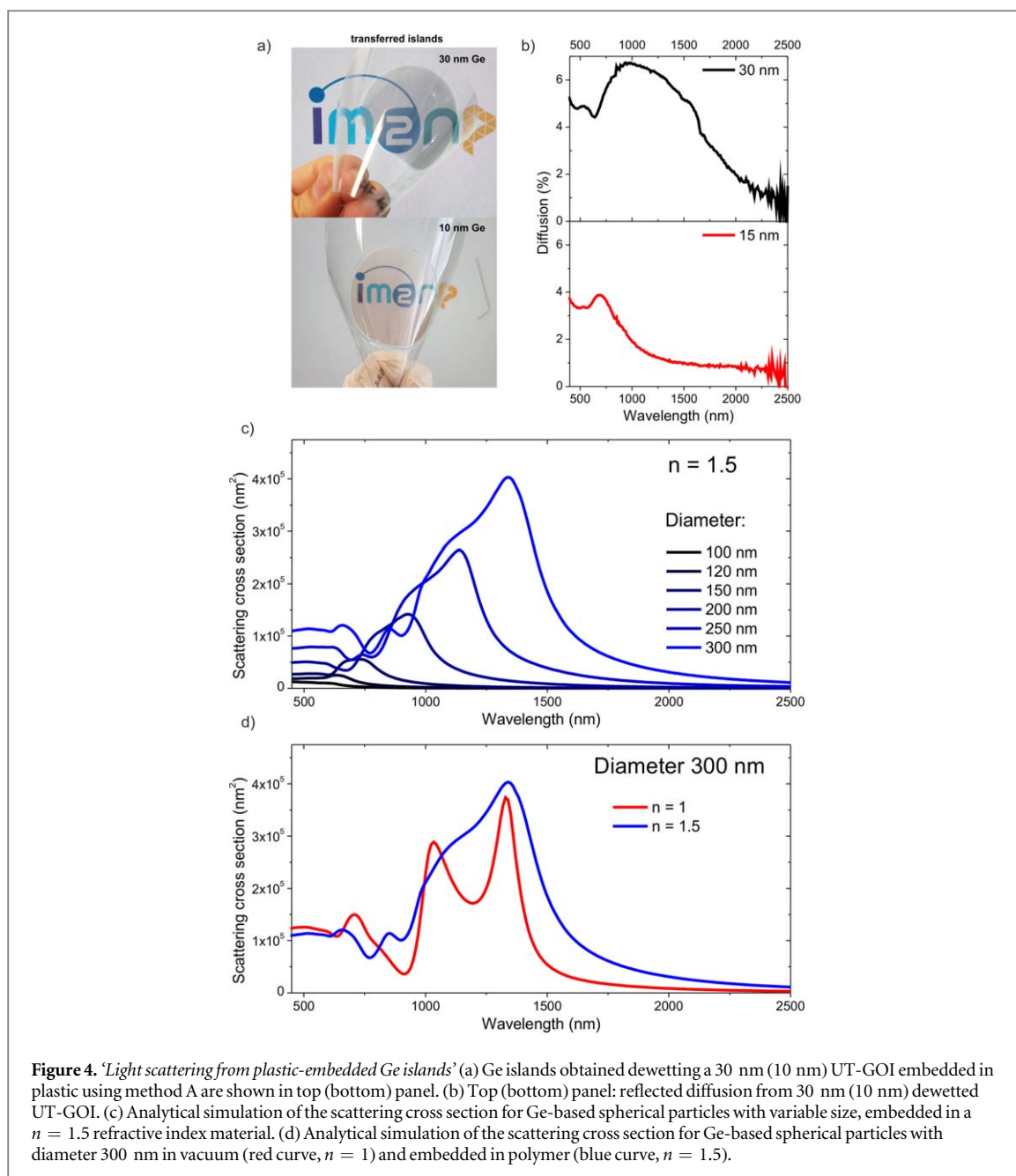
Analytical simulations of the scattering cross section for spherical, Ge-based particles embedded in a $n = 1.5$ refractive index material (that is close to that one of the polymer embedding the Ge islands), are in qualitative agreement with the experimental scattering spectra (figure 4(c)): for 200 nm diameter, Ge-based spherical particles (close to the diameter measured for 30 nm UT-SGOI dewetting, figure 3(d)) we observe a scattering peak at about 900 nm (figure 4(c)). Similar arguments hold for the particles formed from the 10 nm thick UT-GOI.

The origin of the broadening of the measured light scattering is twofold: (1) the ensemble is composed by islands having a rather broad size distribution resulting in a resonant scattering at different wavelength (as shown by the simulation of particles with different size, figure 4(c)), (2) reducing the refractive index contrast between the scatterers and the surrounding medium by embedding the islands in a material with $n = 1.5$ enhances the photon losses affecting the corresponding Q factor of the photonic resonances [39].

3.1. Method B: transfer in PDMS slices

A similar optimization of the island transfer yield, as that one described for method A, was performed for method B (transfer in PDMS, figure 2, bottom panel). This study is conducted on commercial UT-SOI bearing islands sitting on 25 nm thick BOX.
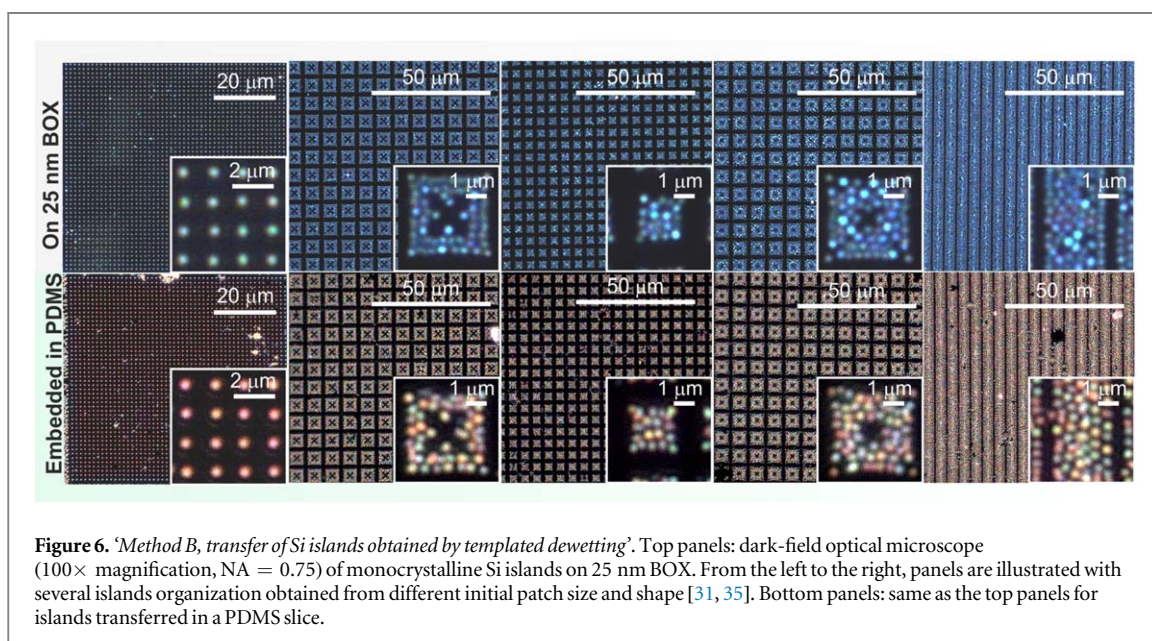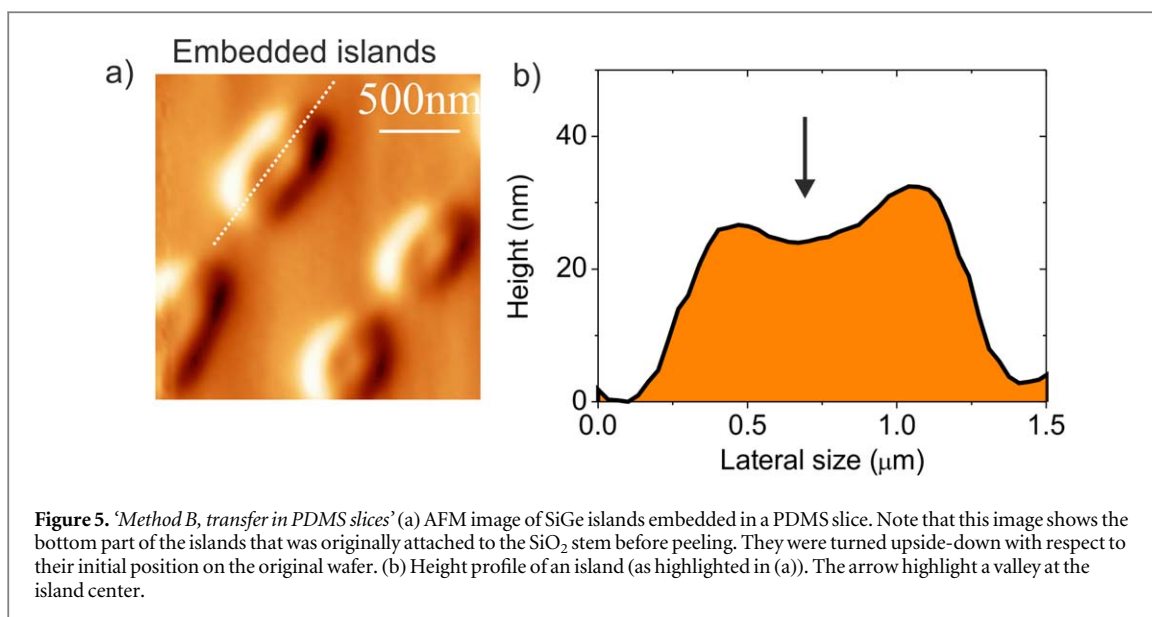
From AFM images, we observe a clear bulging in presence of embedded SiGe islands (figure 5(a)). This feature suggests that the PDMS covering the embedded islands is rather thin, as it is reasonable to expect from

Figure 4. '*Light scattering from plastic-embedded Ge islands*' (a) Ge islands obtained dewetting a 30 nm (10 nm) UT-GOI embedded in plastic using method A are shown in top (bottom) panel. (b) Top (bottom) panel: reflected diffusion from 30 nm (10 nm) dewetted UT-GOI. (c) Analytical simulation of the scattering cross section for Ge-based spherical particles with variable size, embedded in a $n = 1.5$ refractive index material. (d) Analytical simulation of the scattering cross section for Ge-based spherical particles with diameter 300 nm in vacuum (red curve, $n = 1$) and embedded in polymer (blue curve, $n = 1.5$).

the very thin gap left below them when removing the 25 nm thick BOX with HF etching. Furthermore, at the center of the islands' bases, where they were attached to the residual BOX pedestal before transfer, we observe a small valley (less than 10 nm dip, figure 5(b)). Tentatively, we interpret this as the signature of a missing (or very small) residual pedestal attached to the islands' base after transfer.

We now take into account the case of templated dewetting of commercial UT-SOI: [31, 35] by changing the etched patch size and shape (e.g. simple squares, squares with a central cross, parallel trenches) we obtain different arrangement of the Si particles sitting on a 25 nm thick BOX (figure 6 top panels). With a precise organization of individual islands in a square array we can easily count the missing particles in the transferred sample (figure 6 left top and bottom panels). This analysis provides a yield of 99.5% for an HF etching of 20′. Also for complex particles organization the process appears to be almost ideal with the exception of parallel trenches featuring a few dark spots (figure 6 right top and bottom panels).

From the comparison of the islands before and after transfer we observe a remarkable difference in the islands' resonant scattering in optical DF images: when they are on the BOX they all have a similar pale-blue aspect (figure 6, top panels), whereas after transfer, the scattering is brighter and colorful (figure 6, bottom panels), in agreement with similar samples dewetted on a thick BOX [27, 34]. This aspect is addressed more precisely by DF spectroscopy.

Figure 5. *'Method B, transfer in PDMS slices'* (a) AFM image of SiGe islands embedded in a PDMS slice. Note that this image shows the bottom part of the islands that was originally attached to the SiO$_2$ stem before peeling. They were turned upside-down with respect to their initial position on the original wafer. (b) Height profile of an island (as highlighted in (a)). The arrow highlight a valley at the island center.

Figure 6. *'Method B, transfer of Si islands obtained by templated dewetting'*. Top panels: dark-field optical microscope (100× magnification, NA = 0.75) of monocrystalline Si islands on 25 nm BOX. From the left to the right, panels are illustrated with several islands organization obtained from different initial patch size and shape [31, 35]. Bottom panels: same as the top panels for islands transferred in a PDMS slice.

Exploiting low-density samples, where individual islands can be addressed with a confocal microscope, we can directly measure the scattering spectrum of single Si islands on the BOX and embedded in PDMS (figure 7). All these spectra are normalized to the scattering from a Lanbertian reference after subtracting the background. The spectrum of particles on the BOX does not show any resonance and is rather smooth with larger intensity at shorter wavelength, whereas for the transferred ones it features pronounced modulations, as expected for dielectric Mie resonators accounting for the presence of multi-polar resonances (figure 5) [27, 30, 33, 34, 36–38]. Very similar results were obtained for other samples with SiGe and Ge particles transferred in PDMS (not shown).

4. Discussion

From the previous analysis, it emerges that solid state dewetting is extremely well-placed for fabricating sub-micrometric nano-antennas and thus for disordered and ordered dielectric metasurfaces. Nonetheless, one of the main limits of this fabrication method relies in the high-temperature annealing step that impede the formation of high-permittivity islands directly on plastic supports.

Another important need for dewetting is the use of Si wafers having a thickness of a few hundreds micrometers and non-transparent at visible frequencies. This latter feature represents a severe limit of
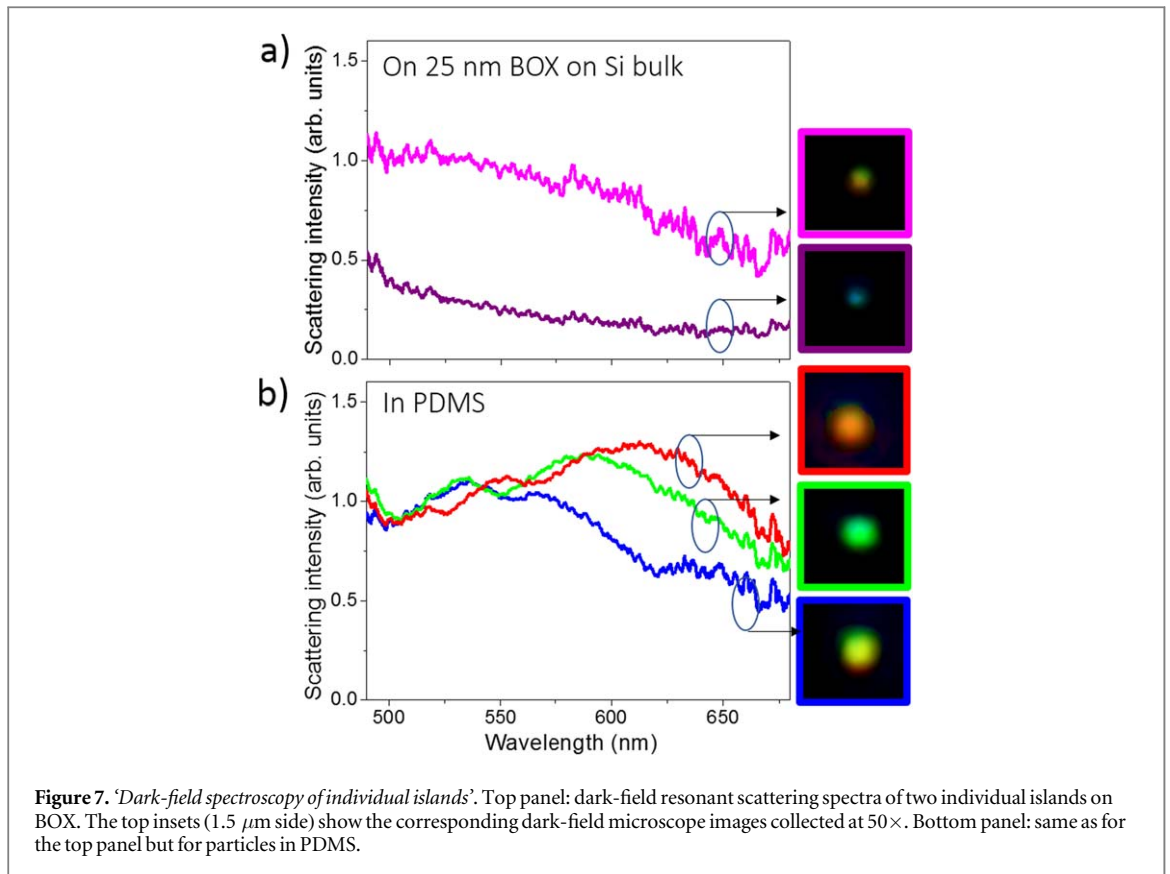
Figure 7. *'Dark-field spectroscopy of individual islands'*. Top panel: dark-field resonant scattering spectra of two individual islands on BOX. The top insets (1.5 μm side) show the corresponding dark-field microscope images collected at 50$\times$. Bottom panel: same as for the top panel but for particles in PDMS.

semiconductor dewetting for light management as for instance, it impedes the use of the final devices for light transmission. Although more robust and transparent supports may be used, such as fused silica or quartz, these materials are expensive and rigid.

Our methods are able to circumvent several of these issues related to solid state dewetting by embedding the islands in transparent and flexible supports. We successfully transferred islands with an almost ideal yield (99.94% for method A and 99.5% for method B) irrespective of their size (from 100 to 500 nm), shape (low vertical aspect ratio of about 1/10 for pure Si to more than 1/2 for Ge-rich islands [27, 28, 34]), composition (from pure Si to pure Ge), density (up to 3 $\times$ 10^9 cm^{-2}), spatial organization (ordered and disordered) and BOX thickness (from 25 to 130 nm).

These features are close to the current state-of-the-art recently reported [24] and in some respect they go beyond. In fact, similar results for dielectric metasurfaces were shown on sacrificial layers of about 100 nm [24] or thicker, bearing particles with larger aspect ratio than what shown here. More generally, the 25 nm thick BOX from commercial UT-SOI we use is by far thinner than other sacrificial layers used for micro- and nano-structure transfer to the best of our knowledge.

We showcased method A on 50 mm wafer, that represents a record for solid state dewetting of group IV materials [33] as well as for bendable dielectric metasurfaces based on Mie resonators (previous reports [24] were implemented on a few mm^2). The merit of our demonstration is also to extend these kind of techniques to SiGe alloys and pure Ge, that are relevant emerging materials for applications in photonics [33, 34] including the important case of integration on plastic supports [40].

Another new aspect of our work is the first demonstration of pronounced and well defined Mie resonances measured on the islands ensemble. Owing to the relatively large size distribution of spontaneously dewetted particles, this latter result was unexpected and is thus extremely promising for realistic applications of SiGe dewetting. In the merit of this, note that, although our devices have been implemented at most over 50 mm wafers, Si wafers are available up to 300 mm (including monocrystalline UT-SOI) accounting for the appeal of our strategy for large-scale, dielectric metasurfaces on transparent supports.

One of the merits of our work relies on the recovered spectral features typical of Mie resonators overcoming the intrinsic limitations of commercial UT-SOI provided with very thin BOX. So far, this latter feature was conveniently exploited to form efficient anti-reflection coatings [33] exploiting the light channeling in the substrate mediated by the Mie resonances [39, 41]. However, when sharp resonances are needed, as for instance for structural color [34], the presence of the high permittivity Si substrate underneath the thin BOX, represents a major limit [39]. In this work, we demonstrated that ordered and disordered arrays of dielectric islands can be

first produced by dewetting, allowing an ultimate control over their size, shape, composition, density and position, and later transferred on low-permittivity, bendable and stretchable supports.

Method A employing MD-700 does not need heating, as the polymer can be reticulated by UV light illumination. In this sense, it is preferable with respect to method B when, for instance, further engineering may be required (e.g. integration of emitting molecules). On the other side, method B exploits PDMS to embed the $Si_{1-x}Ge_x$ islands providing the possibility to stretch them. This option is very attractive and was efficiently exploited for all-optical stress-sensing with dielectric antennas [16].

5. Conclusion

In conclusion, we extended the formation of dielectric islands over 50 mm wafers showing the scalability of our dewetting approach to form dielectric islands and we addressed two different methods for transferring them on low-permittivity supports. The first one is based on MD-700 polymer and adhesive tape, and the second one on PDMS. In both cases the transfer yield can be close to unity for both spontaneous and templated dewetting, providing light and bendable dielectric metasurfaces. In spite of the rather broad size distribution, spontaneously dewetted island provides sufficiently narrow scattering bands to produce a structural color. Thus, the importance of this demonstration relies in the extension of the possible uses of solid state dewetting towards flexible optical devices implemented with an easy and scalable approach.

Acknowledgments

ORCID iDs

Abdennacer Benali ⓘ https://orcid.org/0000-0001-9802-5043
Mohammed Bouabdellaoui ⓘ https://orcid.org/0000-0003-0980-4104
Mimoun Zazoui ⓘ https://orcid.org/0000-0003-2739-628X
Monica Bollani ⓘ https://orcid.org/0000-0002-0078-5085
Marco Salvalaglio ⓘ https://orcid.org/0000-0002-4217-0951
Luc Favre ⓘ https://orcid.org/0000-0002-9010-0085
Marco Abbarchi ⓘ https://orcid.org/0000-0002-2760-4766

References

[1] Loo Y-L, Lang D V, Rogers J A and Hsu J W 2003 *Nano Lett.* **3** 913
[2] Zaumseil J, Meitl M A, Hsu J W, Acharya B R, Baldwin K W, Loo Y-L and Rogers J A 2003 *Nano Lett.* **3** 1223
[3] Thanh Q N, Jeong H, Kim J, Kevek J, Ahn Y, Lee S, Minot E D and Park J-Y 2012 *Adv. Mater.* **24** 4499
[4] Kim D-H, Ghaffari R, Lu N and Rogers J A 2012 *Annu. Rev. Biomed. Eng.* **14** 113
[5] Li L, Lin H, Qiao S, Zou Y, Danto S, Richardson K, Musgraves J D, Lu N and Hu J 2014 *Nat. Photon.* **8** 643
[6] Song D, Secor E B, Wang Y, Hersam M C and Frisbie C D 2018 *ACS Appl. Mater. Interfaces* **10** 22303
[7] Tiefenauer R F, Tybrandt K, Aramesh M and Voros J 2018 *ACS Nano* **12** 2514
[8] Chen Y, Guo Q, Huang G, Li G, Wang L, Tian Z, Qin Y, Di Z and Mei Y 2018 *ACS Appl. Mater. Interfaces* **10** 25644
[9] Zou H *et al* 2017 *Adv. Mater.* **29** 1701412
[10] Zou H *et al* 2019 *ACS Nano* **13** 2289
[11] Hu J, Li L, Lin H, Zhang P, Zhou W and Ma Z 2013 *Opt. Mater. Express* **3** 1313
[12] Li L *et al* 2018 *Light: Sci. Appl.* **7** 17138
[13] Pursiainen O L, Baumberg J J, Ryan K, Bauer J, Winkler H, Viel B and Ruhl T 2005 *Appl. Phys. Lett.* **87** 101902
[14] Lu T-W, Wu C-C, Wang C and Lee P-T 2017 *Opt. Lett.* **42** 2267
[15] Tseng M L, Yang J, Semmlinger M, Zhang C, Nordlander P and Halas N J 2017 *Nano Lett.* **17** 6034
[16] Gutruf P, Zou C, Withayachumnankul W, Bhaskaran M, Sriram S and Fumeaux C 2015 *ACS Nano* **10** 133
[17] Yoo J, Jeong S, Kim S and Je J H 2015 *Adv. Mater.* **27** 1712
[18] Bae S-I, Lee Y, Seo Y-H and Jeong K-H 2019 *Nanoscale* **11** 856
[19] Nie Z and Kumacheva E 2008 *Nat. Mater.* **7** 277
[20] Tang Y, Lin G, Han L, Qiu S, Yang S and Yin J 2015 *Adv. Mater.* **27** 7181

[21] Jalali B and Fathpour S 2006 *J. Lightwave Technol.* **24** 4600
[22] Smit M, Leijtens X, Bente E, van der Tol J, Ambrosius H, Robbins D, Wale M, Grote N and Schell M 2012 *OFC/NFOEC* (Piscataway, NJ: IEEE) pp 1–3
[23] Chanda D, Shigeta K, Gupta S, Cain T, Carlson A, Mihi A, Baca A J, Bogart G R, Braun P and Rogers J A 2011 *Nat. Nanotechnol.* **6** 402
[24] Kamali S M, Arbabi A, Arbabi E, Horie Y and Faraon A 2016 *Nat. Commun.* **7** 11618
[25] Zhang J, Haq B, Oallaghan J, Gocalinska A, Pelucchi E, Trindade A J, Corbett B, Morthier G and Roelkens G 2018 *Opt. Express* **26** 8821
[26] Thompson C V 2012 *Annu. Rev. Mater. Res.* **42** 399
[27] Abbarchi M, Naffouti M, Vial B, Benkouider A, Lermusiaux L, Favre L, Ronda A, Bidault S, Berbezier I and Bonod N 2014 *ACS Nano* **8** 11181
[28] Naffouti M, David T, Benkouider A, Favre L, Ronda A, Berbezier I, Bidault S, Bonod N and Abbarchi M 2016 *Nanscale* **8** 7768
[29] Naffouti M, David T, Benkouider A, Favre L, Delobbe A, Ronda A, Berbezier I and Abbarchi M 2016b *Small* **12** 6115
[30] Naffouti M, David T, Benkouider A, Favre L, Cabie M, Ronda A, Berbezier I and Abbarchi M 2016c *Nanotechnology* **27** 305602
[31] Naffouti M *et al* 2017 *Sci. Adv.* **3** eaao1472
[32] Zhang P, Yang B, Rugheimer P, Roberts M, Savage D, Liu F and Lagally M 2009 *J. Phys. D: Appl. Phys.* **42** 175309
[33] Bouabdellaoui M *et al* 2018 *Phys. Rev. Mater.* **2** 035203
[34] Wood T *et al* 2017 *ACS Photonics* **4** 873
[35] Abbarchi M *et al* 2018 *Microelectron. Eng.* **190** 1
[36] Evlyukhin A B, Reinhardt C and Chichkov B N 2011 *Phys. Rev. B* **84** 235429
[37] García-Etxarri A, Gómez-Medina R, Froufe-Pérez L S, López C, Chantada L, Scheffold F, Aizpurua J, Nieto-Vesperinas M and Sáenz J J 2011 *Opt. Express* **19** 4815
[38] Coenen T, van de Groep J and Polman A 2013 *ACS Nano* **7** 1689
[39] van de Groep J and Polman A 2013 *Opt. Express* **21** 26285
[40] Zhu X, Yan W, Levy U, Mortensen N A and Kristensen A 2017 *Sci. Adv.* **3** e1602487
[41] Spinelli P, Verschuuren M and Polman A 2012 *Nat. Commun.* **3** 692